In situ time-resolved measurements of carbon nanotube and nanohorn growth

D. B. Geohegan[*], **A. A. Puretzky, D. Styers-Barnett, H. Hu, B. Zhao, H. Cui, C. M. Rouleau, G. Eres, J. J. Jackson, R. F. Wood, S. Pannala,** and **J. C. Wells**

Oak Ridge National Laboratory, Oak Ridge, TN 37831, USA

Growth mechanisms of carbon nanotubes are investigated and compared for both high- and low-temperature synthesis methods through experiments utilizing time-resolved, *in situ* imaging and spectroscopy. High-speed videography and pyrometry measured the timeframes for growth for single-wall carbon nanotubes (SWNTs) and nanohorns (SWNHs) by laser vaporization (LV) at 1150 °C, revealing that C can self-assemble at high temperatures preferentially into SWNH structures without catalyst assistance at rates comparable to catalyst-assisted SWNT growth by either laser vaporization or chemical vapor deposition (CVD). Laser interferometry and videography reveal the coordinated growth of vertically-aligned nanotube arrays (VANTAs) by CVD at 550–900 °C.

1 Introduction

The mechanisms of carbon nanotube nucleation and growth remain the subject of much research interest from both fundamental and applied perspectives. Recently, *in situ* environmental electron microscopy investigations of nanotube synthesis have provided glimpses of their growth processes [1, 2] however many questions remain unanswered. Specifically: (1) The timeframes and energetics for nucleation. (2) The feedstocks for growth in both high- and low-temperature nanotube synthesis. (3) The state of the metal nanoparticle during growth in both high and low-temperature synthesis methods. (4) Whether carbon dissolves and diffuses through the metal catalyst nanoparticle to grow a nanotube, or whether nanotubes grow from complex surface chemistry on a metal nanoparticle. (5) The factors which determine the diameter, chirality, and numbers of walls of a nanotube. (6) The roles of hydrogen and intermediate gas phase reactions in sustaining growth. (7) The mechanisms for growth termination. (8) Whether growth can be stopped and restarted after catalyst poisoning. (9) The roles of the catalyst support on the chirality of the resulting nanotube [3]. *In situ* characterization of both the growth environment and the characteristics of the catalyst particle and the nanotube (e.g. length, diameter, number of walls, structure) are being developed to help answer these questions. Together with control over the synthesis conditions (pressure, flow, temperature), models of nanotube growth can be developed and tested. This paper illustrates two such techniques which have applications in the nanoengineering of loose SWNHs with variable morphology to explore hydrogen storage [4], and the controllable growth of VANTAs as thermal conductors [5].

[*] Corresponding author: e-mail: geohegandb@ornl.gov

phys. stat. sol. (b) **244**, No. 11 (2007)
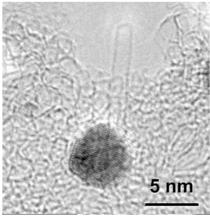
3945

2 Experimental

Laser vaporization of carbon targets containing ~1–2 at% metal catalyst powders (e.g. Ni and Co) is a very effective technique to produce exclusively SWNTs at ~1200 °C in flowing Ar [6]. *In situ* imaging and spectroscopy studies of the ns-laser vaporization process revealed that (a) both carbon and metal are prinicpally in the form of atoms and molecules (C, C_2, C_3, Ni, Co) during the first 100 µs, when the plume of ejecta are within ~1 cm of the target, (b) that carbon forms clusters within 1 ms after laser vaporization, as the hot plasma cools, and that (c) Ni and Co form clusters later in time (1 ms $< t <$ 2 ms) after laser ablation [7, 8]. Through stop-growth experiments, where the plume was ejected from the hot oven after different growth periods (as revealed by imaging the plume via Rayleigh scattering), it was learned that only short SWNT "seeds" or nuclei had formed after 15–20 ms of growth time (see Fig. 1). By adjustment of this time, a growth rate in the range of 1–5 microns/second could be inferred for SWNT growth by laser vaporization [9].

Recently, we have employed a variable pulse-width laser (Nd:YAG, 1.06 µm, 600 W average power, 10 000 W peak power, adjustable pulse width >0.5 ms, 500 Hz maximum repetition rate). The significantly longer pulses provide opportunities for high plasma plume temperatures to be maintained for adjustable time periods, as measured by high-speed videography and pyrometry. Moreover, the energy can be distributed among many low-energy pulses which accumulate energy on the target for *cumulative* laser vaporization (e.g. one hundred 1 ms, 1 J pulses) or high-energy, long single pulses for *continuous* laser vaporization (e.g. one 10 ms, 100 J pulse). Single-wall carbon nanohorns are single-walled carbon nanostructures which can be grown by laser or arc vaporization into room-temperature ambients without the aid of metal catalysts [10]. The mechanisms for their growth are unclear. Here we report SWNH growth at oven temperatures identical to those used for SWNT synthesis, and explore the range of optimal laser pulse widths and energies for both SWNTs and SWNHs.

To study nucleation and growth processes *in situ* during chemical vapor deposition (CVD) time-resolved reflectivity (TRR) [11] from vertically-aligned nanotube arrays (VANTAs) and direct videography [12] are employed. In TRR, Fabry−Perot interference fringes are recorded on a photodiode from a He−Ne laser beam which is reflected both from the top of the VANTA array and from the portion of the beam which penetrates the array and is reflected from the (typically Si) substrate. The substrate is typically coated with an evaporated Al (10 nm) film onto which metal catalyst films (typically 0.5−1.0 nm of Fe or Fe/Mo) are electron-beam evaporated. For videography, a video camera and remote microscope are used to directly image the forest of nanotubes with ~10 micron resolution.

3 Results

To explore SWNT and SWNH growth by LV, sets of C targets were fabricated utilizing Dylon cement as described previously, both with and without metal catalyst powders [6−8]. The yield and morphology of
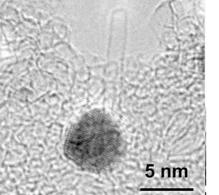

Fig. 1 HRTEM of a short SWNT emanating from a NiCo catalyst particle grown by time-restricted growth within a 1150 °C tube furnace following ns-laser vaporization.
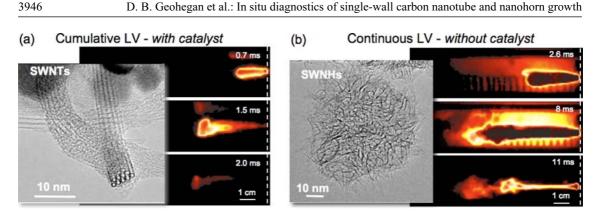
Fig. 2 (online colour at: www.pss-b.com)   Selected frames from video images recorded *in situ* from within a 1150 °C tube furnace during high-power laser vaporization of (a) a C target containing 1 at% each of Ni and Co used to make SWNTs in the *cumulative* mode (1 ms, 9 J laser pulses) and (b) a pure C target used to make SWNHs in the *continuous* mode (10 ms, 90 J laser pulses). Variation of the laser pulse widths and energies can be used to adjust the times and temperatures available for single-wall carbon nanotube and nanohorn growth. HRTEM images show representative materials collected outside the furnace following the synthesis events illustrated by the time-resolved image sequences.

SWNTs and SWNHs produced at different laser pulse widths and energies were examined by HRTEM, Raman spectroscopy, and SEM and compared to the target temperatures measured by *in situ* optical pyrometry and the plume cooling times measured by *in situ* videography (measured with a 50,000 frame-per-second video camera). The detailed study will be the subject of a separate publication [11].

Only SWNHs were produced from the catalyst-free targets with the individual nanohorn length and aggregate diameter increasing with increasing pulse width. In general with the catalyst-loaded targets, SWNHs and SWNTs were generally co-synthesized at most pulse widths. Only by minimizing laser pulse width and pulse energy could observable SWNHs be eliminated. Figure 2 illustrates the plume conditions for high-yield SWNT and SWNH growth by cumulative LV of catalyst-loaded targets, and continuous LV of catalyst-free targets, respectively. Selected false-color images from the videos show the extent and visible plasma emission of the laser plume from the target surface (dashed line position).

For SWNTs in Fig. 2(a), plume formation and thermalization to oven temperature occurs within <4 ms. This *cumulative* mode of laser ablation utilizes preheating of the target from prior laser pulses to enable efficient vaporization from successive pulses. For SWNHs, longer *continuous* laser pulses with high energy as in Fig. 2(b) were found to be most successful by prolonging high plasma temperatures and thermalization times to ~30 ms. From HRTEM analysis, the length of the SWNH subunits within the nanohorn aggregates was estimated to increase ~1 nm for each additional millisecond of growth time above oven temperature. Thus, C is capable of self-assembling into single-wall carbon structures at 1 µm/s rates, very similar to rates measured for catalyst-assisted assembly in both LV and CVD processes.

To understand the growth kinetics of nanotubes during CVD, TRR and videography of VANTAs permits a wide variety of phenomena to be explored [12, 13]. For example, Fig. 3 shows VANTA growth at 575 °C and the effects of laser irradiation on the growth rate. At $t = 60$ s after initiation of growth, a pulsed Nd:YAG laser running at 10 Hz ($\lambda = 1.064$ µm, 0.6 J/cm^2 fluence, 10 Hz) irradiates the growing VANTA, resulting in a rapid change in the average growth rate of the array (likely due to laser heating). Each fringe oscillation corresponds to ~0.3 µm of array height, which permits an average length and growth rate to be estimated. Note that the lengths measured are those for the array as a whole, and reflect the overall growth kinetics of nanotubes growing in a coordinated (and not necessarily straight) fashion.

Through careful control over the catalyst composition, feedstock supply, and temperature, very high fractions of SWNTs in VANTAs can be grown [14, 15]. According to the growth models developed from measurements of growth rates and terminal lengths of VANTAs at different feedstock flow rates
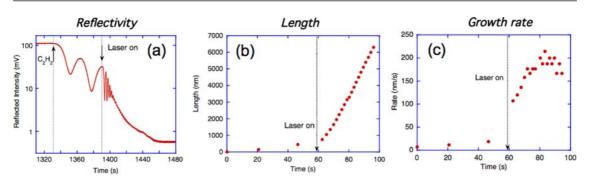
Fig. 3 (online colour at: www.pss-b.com)   Time-resolved reflectivity recorded *in situ* from a growing vertically-aligned nanotube array. (a) Fabry–Perot oscillations and exponential drop in signal intensity start within seconds following the introduction of acetylene, and increase in frequency due to laser irradiation 60 s later. (b) Length and (c) growth rate analyzed from the oscillations in (a) permit the kinetics of growth under different conditions to be analyzed within a given growth run.

and substrate temperatures, the growth rate, terminal length, and the number of walls of the nanotubes grown within a VANTA array can be predicted [16, 17]. The models predict that a SWNT is the fastest growing nanotube at a given temperature, and that oversupply of C beyond that required to grow a SWNT will result in nanotubes with additional walls, not an increase in growth rate [17]. To illustrate this effect, the growth conditions can be changed during a run under *in situ* reflectivity monitoring. Figure 4 illustrates Raman spectra from a VANTA array initially growing with a high fraction of SWNTs as evidenced by a strong SWNT RBM mode and high Raman G/D band ratio. Arrays with high and nearly constant SWNT fractions can be grown as shown in Fig. 4(c) and since the nanotubes grow from catalyst particles at their bases, the nanotubes at the top of the array are the first grown. Abruptly changing the feedstock supply from 1 sccm to 10 sccm shifts the growth conditions from SWNTs to MWNTs in accordance with the growth models, as evidenced by changes in the Raman spectra in Figs. 4(b) and (c).

Videography reveals regional kinetics information not observed by TRR. As shown in Fig. 5, time-lapse videography of VANTAs shows that initially the arrays grow rapidly and very uniformly. How-
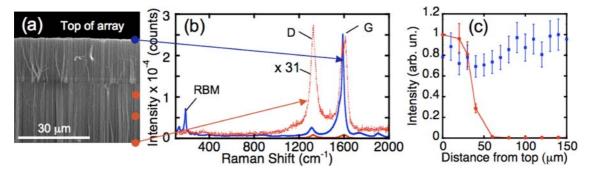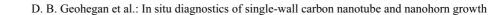

Fig. 4 (online colour at: www.pss-b.com)   (a) SEM image of the top of a VANTA array grown with different partial pressures of acetylene at 760 Torr, 750 °C in 2500 sccm Ar/H_2 gas mixture. Since the nanotubes grow from catalyst anchored at the substrate, the top of the array (grown with 1 sccm C_2H_2) reflects nanotubes which grew first, and display a high SWNT fraction displaying (b) Raman spectra (λ_{ex} = 633 nm) with pronounced RBM modes and a high G/D Raman band ratio (blue curve). The number of walls in the array can be adjusted, in accordance with the growth model, by an oversupply in feedstock. Thus, the bottom part of the array (grown with 10 sccm C_2H_2) displays a lack of SWNTs and a Raman spectrum reflecting MWNTs (red curves, actual intensity and scaled by a factor of 31). (c) Raman profiling of the array (laser polarization parallel to the nanotube alignment) shows a drop-off in RBM intensity (red circles and line) following the change to 10 sccm feedstock supply after 15 microns of initial growth. An array grown at 1 sccm constant supply (blue square points) is shown for comparison.
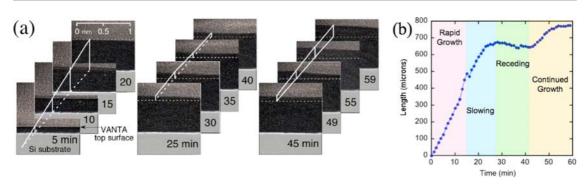
Fig. 5 (online colour at: www.pss-b.com)   (a) Video images recorded *in situ* from vertically-aligned nanotube array growing from flowing $C_2H_2/H_2/Ar$ within a 730 °C tube furnace from a Mo(0.2 nm)/Fe(1 nm)/Al(10 nm) coated Si-substrate. Regional variations across the ~1 mm field-of-view show a coordinated growth behavior. (b) Plot of the VANTA height at the indicated position (white lines) in (a) illustrates a region of rapid growth, slowing, *retraction,* resumption, and termination of growth during the 60 minute period.

ever, regional instabilities in growth rate are observed concurrent with slowing of the growth rate. At certain points in the array, the height is actually observed to recede. This instability normally signals the onset of growth termination, however as shown in Fig. 5(b) in many cases the the array height undergoes another increase in length before the nanotubes terminate growth.

4   Conclusions

In situ imaging and pyrometry of the LV processes resulting in SWNT and SWNH growth indicate that both processes proceed at nearly equal rates of ~1 μm/s of available growth time. In the *catalyst-free* growth of SWNHs from pure C, maintenance of high plasma temperatures through *continuous* laser vaporization is essential. Molecular dynamics simulations have shown that the formation of curved carbon structures (such as fullerenes) from atomic and molecular constituents require vibrational temperatures above 2500 K [18], in agreement with our findings. By contrast, SWNTs grow at extended times to microns in length following plume thermalization to the oven temperature, from *catalyst-assisted* consumption of carbon fragments synthesized by *cumulative* laser vaporization with pulse widths <1 ms. The finding that SWNTs and SWNHs can form together at intermediate pulse widths and laser energies indicate that the precursors for SWNH growth are compatible with catalyst-assisted SWNT growth by condensed phase conversion.

Time-resolved reflectivity and videography of VANTA growth by CVD permits direct nanotube growth kinetics measurements for the development of growth models. As shown here, these techniques also provide methods to understand modifications to the growth environment, such as growth rate changes caused by laser-induced temperature increases or feedstock flow adjustments. Videography of VANTA synthesis shows cooperative phenomena which tend to equilibrate the height of the arrays over lateral distances of several millimeters. Observations of the array heights vs. time show that local regions of the array appear to have variable growth rates, i.e., pausing, resuming, and even retracting significantly during a growth run. The retraction of the array may be caused by tension resulting from kinking or entanglement of nanotubes which have different growth rates, possibly explaining the coordinated growth behavior. Sharma, et al. have observed pauses in the growth of nanotubes during *in situ* TEM studies, with different nanoparticles switching 'on' and 'off' according to highly localized favorable or unfavorable growth conditions [19]. Tension in the array, or localized feedstock depletion, may provide sufficient impetus for such growth spurts in the coordinated growth witnessed here. At a minimum, the measured heights vs. time reflect both the growth and the retraction of the nanotubes in the array. Further *in situ* experiments are required to elucidate the forces inherent in coordinated growth, the evolution of tension in the arrays and its possible feedback on the activity of the catalyst.

References

[1] S. Helveg, C. Lopez-Cartes, J. Sehested, P. L. Hansen, B. S. Clausen, J. R. Rostrup-Nielsen, F. Abild-Petersen, and J. K. Norskov, Nature **427**, 426 (2004).

[2] S. Hoffman et al., this conference.

[3] NASA/Rice SWNT Growth Mechanisms Workshop Rapporteur report, Burnet, Texas (2007).

[4] F. Fernandez-Alonso, F. J. Bermejo, C. Cabrillo, R. O. Loutfy, V. Leon, and M. L. Saboungi, Phys. Rev. Lett. **98**, 215503 (2007).

[5] I. N. Ivanov, A. A. Puretzky, G. Eres, H. Wang, Z. W. Pan, H. T. Cui, R. Y. Jin, J. Howe, and D. B. Geohegan, Appl. Phys. Lett. **89**, 223110 (2006).

[6] T. Guo, P. Nikolaev, A. Thess, D. T. Colbert, and R. E. Smalley, Chem. Phys. Lett. **236**, 419 (1995).

[7] A. A. Puretzky, D. B. Geohegan, X. Fan, and S. J. Pennycook, Appl. Phys. Lett. **76**, 182, (2000).

[8] A. A. Puretzky, D. B. Geohegan, X. Fan, and S. J. Pennycook, Appl. Phys. A **70**, 153, (2000).

[9] A. A. Puretzky, H. Schittenhelm, X. Fan, M. J. Lance, L. F. Allard, Jr., and D. B. Geohegan, Phys. Rev. B **65**, 245425 (2002).

[10] S. Iijima, M. Yudasaka, R. Yamada, S. Bandow, K. Suenaga, F. Kokai, and K. Takahashi, Chem. Phys. Lett. **309**, 165, (1999).

[11] D. B. Geohegan, H. Hu, A. A. Puretzky, B. Zhao, D. Styers-Barnett, and C. M. Rouleau (in preparation).

[12] D. B. Geohegan, A. A. Puretzky, I. N. Ivanov, S. Jesse, G. Eres, and J. Y. Howe, Appl. Phys. Lett. **83**, 1851 (2003).

[13] A. A. Puretzky, G. Eres, C. M. Rouleau, I. N. Ivanov, and D. B. Geohegan (submitted).

[14] K. Hata, D. N. Futaba, K. Mizuno, T. Namai, M. Yumura, and S. Iijima, Science **306**, 1362 (2004).

[15] G. Eres, A. A. Kinkhabwala, H. Cui, D. B. Geohegan, A. A. Puretzky, and D. H. Lowndes J. Phys. Chem. B **109**, 16684–16694 (2005).

[16] A. A. Puretzky, D. B. Geohegan, S. Jesse, I. N. Ivanov, and G. Eres, Appl. Phys. A **81**, 223 (2005).

[17] R. F. Wood, S. Pannala, J. C. Wells, A. A. Puretzky, and D. B. Geohegan, Phys. Rev. B, **75** 235446 (2007).

[18] Y. Yamaguchi and S. Maruyama, Chem. Phys. Lett., **286**, 336 (1998).

[19] R. Sharma, P. Rez, M. M. J. Treacy, and S. J. Stuart, J. Electron. Microsc. **54**, 231 (2005).